MIT OpenCourseWare
http://ocw.mit.edu

Electromechanical Dynamics

For any use or distribution of this textbook, please cite as follows:

Woodson, Herbert H., and James R. Melcher. *Electromechanical Dynamics*.
3 vols. (Massachusetts Institute of Technology: MIT OpenCourseWare).
http://ocw.mit.edu (accessed MM DD, YYYY). License: Creative Commons
Attribution-NonCommercial-Share Alike

For more information about citing these materials or
our Terms of Use, visit: http://ocw.mit.edu/terms

Chapter 14

ELECTROMECHANICAL COUPLING WITH VISCOUS FLUIDS

14.0 INTRODUCTION

In Chapters 12 and 13 mathematical descriptions of lossless fluids are presented in a study of several basic types of electromechanical interaction with fluids. In the introductory section (12.0) of Chapter 12, we indicated that viscosity can have some marked effects on electromechanical interactions, especially when the system involves the flow of a fluid near a solid boundary. In this chapter the earlier fluid models are generalized to include the effects of fluid mechanical losses (viscosity), and the generalized models are used to study the effects of viscosity on some electromechanical interactions.

In our considerations of viscosity we limit our attention to incompressible fluids. The viscous effects we shall study also occur in compressible fluids, and the incompressible model we shall use is often employed to estimate the effects of viscosity on the flow of compressible fluids. Nonetheless, our model does not include mechanical losses due to longitudinal (dilatational) distortion of the fluid, and thus it is inadequate for a study of the effects of viscosity on longitudinal disturbances such as acoustic and magnetoacoustic waves. At the appropriate point in the development we indicate how the necessary extension can be made.

Our model for viscous fluids is restricted to *Newtonian fluids* whose stress-strain rate relations are linear. This model is a good representation of most fluids of interest in electromechanical interactions. It is analogous to the model of a linear resistance in electric circuits. Non-Newtonian fluids require suitable nonlinear models.*

* R. R. Long, *Mechanics of Solids and Fluids*, Prentice-Hall, Englewood Cliffs, N.J., 1961, pp. 69–72.

14.1   VISCOUS FLUIDS

In Section 12.1.4 the mechanical interaction force between adjacent fluid
particles in an inviscid fluid is represented by the hydrostatic pressure p.
When a viscous fluid is at rest, the mechanical interaction of adjacent
particles is still described by a hydrostatic pressure. With the fluid in motion,
it is subjected to pressure forces just as an inviscid fluid is, but, in addition,
there is a force due to friction between adjacent particles that are in relative
motion. The effects of this friction force are accounted for mathematically
by defining a fluid *viscosity*.

14.1.1   Mathematical Description of Viscosity

A simple, one-dimensional example helps to introduce a derivation of the
stress-tensor (hence force density) that represents the fluid friction.† Figure
14.1.1 shows a viscous fluid contained between parallel plates. We can
imagine such a situation in which the system has large dimensions in the x_1-
and x_3-directions. The plates are set into steady relative motion by externally
applied forces. The viscous fluid near the upper plate tends to move with it.
Similarly, the fluid at $x_2 = 0$ tends to move with the lower plate. Forces have
to be applied to the two plates to maintain relative motion and, when steady-
state conditions exist, there must be equal and opposite forces acting on the
two plates, as indicated in Fig. 14.1.1. If each plate has the area A, there is a
shear stress (force per unit area), given by
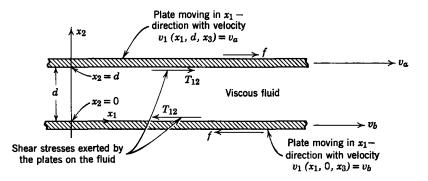
$$T_{12} = \frac{f}{A}. \tag{14.1.1}$$

Fig. 14.1.1   Simple example of shear flow.

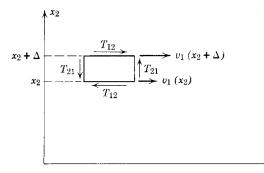† This example is considered in more detail in Section 14.1.3.

Fig. 14.1.2   Equilibrium for a small element of fluid of thickness Δ.

Experiments show that for a variety of fluids the shear stress T_{12} applied to the fluid by the plates is directly proportional to the difference of the plate velocities and inversely proportional to the plate spacing d:

$$T_{12} = \mu \left(\frac{v_a - v_b}{d} \right). \qquad (14.1.2)$$

The constant of proportionality μ is defined as the *coefficient of viscosity*. This constant μ describes a Newtonian fluid. A non-Newtonian fluid does not exhibit the linear relation between velocity difference and shear stress.

An experiment of this kind leads us to postulate that for a certain type of fluid flow an element of fluid of infinitesmal thickness, shown in Fig. 14.1.2, is held in equilibrium by the shear stress T_{12}, where

$$T_{12} = \lim_{\Delta \to 0} \mu \left[\frac{v_1(x_2 + \Delta) - v_1(x_2)}{\Delta} \right] = \mu \frac{\partial v_1}{\partial x_2}. \qquad (14.1.3)$$

Moreover, because the torque on the infinitesmal element must be zero,

$$T_{21} = T_{12}. \qquad (14.1.4)$$

From (8.1.10)* we conclude that the force density due to viscosity in our simple one-dimensional problem is

$$F_1 = \mu \frac{\partial^2 v_1}{\partial x_2{}^2}. \qquad (14.1.5)$$

Because the motion is steady and the pressure is uniform, this force density F_1 must be zero. Two boundary conditions are then required to integrate (14.1.5). Our intuition tells us that the fluid moves with (sticks to) a contiguous boundary; for example, in Fig. 14.1.1 the constants are determined by the conditions that

$$v_1(d) = v_a,$$
$$v_1(0) = v_b,$$

* See Table 8.1, Appendix G.

and it follows that

$$v_1 = \frac{(v_a - v_b)}{d}\, x_2 + v_b.$$

Of course, the force density and stress tensor deduced are of limited validity. The steps outlined, however, serve to indicate the approach that is now used to establish a stress tensor of more general validity. The similarity of this example and the one-dimensional elasticity problem of Section 9.1* suggest that we approach the problem of deriving the viscous stresses by the same techniques that were used to find the elastic stress tensor. Equation 14.1.3 emphasizes the basic difference between fluid and elastic media. Rather than a linear relation between stress and strain, as we found in dealing with elastic media [see (11.2.32)], we now find a linear relation between stress and *rate of strain*. Hence we can establish the viscous stress tensor in two steps: first, we relate the velocity to the rate of strain, which is defined in a way analogous to that in Section 11.2.1 for strain, and, second, we introduce the empirical relationship between stress and the rate of strain. We can then find the force density from the stress tensor by simply taking the divergence of the stress tensor (8.2.7)†.

14.1.1a The Strain-Rate Tensor

The strain-rate tensor, like the strain tensor, is defined by geometrical considerations. It is defined in such a way that its components represent those types of fluid flow that would be expected to give rise to a viscous stress. Because the relation between stress and strain rate (as found in the laboratory) is linear, it is possible to superimpose various types of deformation rates to describe an arbitrary deformation rate. Our development now parallels that used in connection with the strain tensor which described elastic media (Section 11.2.1).

A one-dimensional flow, such as that used to introduce this section, is shown in Fig. 14.1.3*a*. If we now consider the flow in the neighborhood of point A, the velocity field may be divided into a pure translation, as shown in Fig. 14.1.3*b*, and the flow of Fig. 14.1.3*c*. A pure translation cannot give rise to a viscous stress, for the particles that interact with those at A from above or below or to the right or left are moving at the same velocity as those at point A.

Now, in turn, we can divide the remaining flow field into two parts, as shown in Fig. 14.1.4. There is now a part that represents a rigid-body rotation about point A and a part that we call a *shear flow*. Viscous stresses would not be expected to arise from rigid-body rotation any more than they would from rigid-body translation. Hence a flow with the character of that shown in Fig. 14.1.4*c* must be related to the viscous stress.
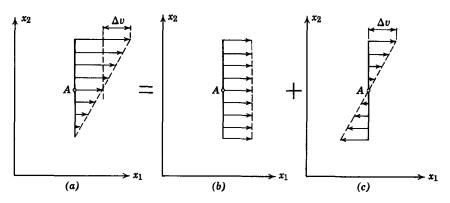
* See Table 9.2, Appendix G.

† Appendix G.

Fig. 14.1.3 Decomposition of flow into rigid-body translation of point A and flow with respect to that point.

It is worthwhile to recall the attributes of a flow field $v(x_1, x_2, x_3, t)$ that correspond to rotation. Clearly, if fluid is rotating about point A, the line integral of v along a contour C that encloses point A is some finite number, say Γ.

$$\oint_C \mathbf{v} \cdot d\mathbf{l} = \int_S (\nabla \times \mathbf{v}) \cdot \mathbf{n} \, da = \Gamma. \tag{14.1.6}$$

We have used Stokes's theorem to transform the line integral to an integral over the surface enclosed by the contour C. From (14.1.6) it is apparent that the magnitude of the rotation about a point is proportional to $\nabla \times \mathbf{v}$. For the simple flow field shown in Figs. 14.1.3 and 14.1.4 there is only an i_3-component of the curl, and that is

$$(\nabla \times \mathbf{v})_3 = \left(\frac{\partial v_2}{\partial x_1} - \frac{\partial v_1}{\partial x_2} \right). \tag{14.1.7}$$
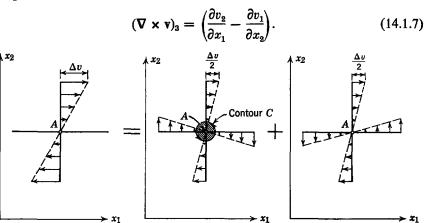

Fig. 14.1.4 Decomposition of flow into rotation and shear components: (a) total flow with respect to point A; (b) rigid-body rotation; (c) shear flow,

In our one-dimensional example we found that the stress T_{12} is proportional to $\partial v_1/\partial x_2$ [see (14.1.3)]. We can however, write this derivative as

$$\frac{\partial v_1}{\partial x_2} = \frac{1}{2}\left(\frac{\partial v_1}{\partial x_2} - \frac{\partial v_2}{\partial x_1}\right) + \frac{1}{2}\left(\frac{\partial v_1}{\partial x_2} + \frac{\partial v_2}{\partial x_1}\right), \qquad (14.1.8)$$

and we see that it includes the rotation of (14.1.7). Equation 14.1.8 is the analytical representation of Fig. 14.1.4. Our point is that it is reasonable to define as the component of the *shear rate* $\dot{e}_{12}$

$$\dot{e}_{12} = \frac{1}{2}\left(\frac{\partial v_1}{\partial x_2} + \frac{\partial v_2}{\partial x_1}\right), \qquad (14.1.9)$$

since it represents the only part of the deformation rate that is not (locally) a rigid-body translation or rotation. From the symmetry of the x_1- and x_2-coordinates it follows that $\dot{e}_{12} = \dot{e}_{21}$. Although our remarks have been made for flow fields in the x_1-x_2-plane, they apply equally well with other combinations of the coordinates. Hence we define

$$\dot{e}_{ij} = \frac{1}{2}\left(\frac{\partial v_i}{\partial x_j} + \frac{\partial v_j}{\partial x_i}\right). \qquad (14.1.10)$$

Although so far we have discussed the situation in which $i \neq j$ in (14.1.10), those components given by $i = j$ also represent a rate of deformation that was not present in our simple example. If $\nabla \cdot \mathbf{v} \neq 0$, it is possible for the fluid to execute a motion of the kind illustrated in Fig. 14.1.5*b*. There the fluid in the region of the point A is either expanding or contracting. We can characterize this dilatational motion by the three terms of the divergence, recognized as $\dot{e}_{ij}$ when $i = j$. The mechanism by which a dilatational motion can produce a viscous stress is not defined by the simple experiment discussed in the introduction to this section It is therefore not surprising that we find it necessary to define (and measure by some other means than a shear flow) a second coefficient of viscosity. It is important to recognize that the strain-rate, *defined* by (14.1.10), unlike the strain *approximated* by (11.2.10), involves no approximations about magnitudes of motion.

We can arrive at our definition of the strain-rate tensor in a more precise fashion by considering the relative velocity of fluid at two adjacent points in the flow field. For this purpose we define two points in a cartesian coordinate system which are at $\mathbf{r}$ and $\mathbf{r} + \Delta\mathbf{r}$, where

$$\mathbf{r} = \mathbf{i}_1 x_1 + \mathbf{i}_2 x_2 + \mathbf{i}_3 x_3 = \mathbf{i}_i x_i,$$

$$\Delta\mathbf{r} = \mathbf{i}_1 \, \Delta x_1 + \mathbf{i}_2 \, \Delta x_2 + \mathbf{i}_3 \, \Delta x_3 = \mathbf{i}_i \, \Delta x_i.$$
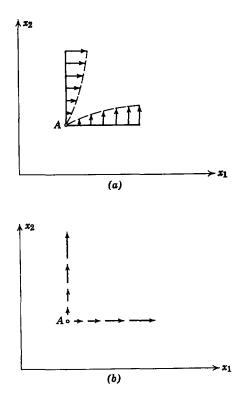
These coordinate vectors are shown in Fig. 14.1.6.

Fig. 14.1.5 Illustration of shear and dilatation at point A: (a) shear; (b) dilatation.
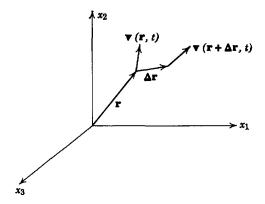

Fig. 14.1.6 System for defining rate of strain.

To find the velocity of the particle at $\mathbf{r} + \Delta\mathbf{r}$ with respect to the particle at $\mathbf{r}$ we expand the velocity in a Taylor series about the coordinate $\mathbf{r}$ and (because we are interested only in the region near $\mathbf{r}$) keep only linear terms. For the ith component we obtain

$$\Delta v_i = v_i(\mathbf{r} + \Delta\mathbf{r}, t) - v_i(\mathbf{r}, t) = \frac{\partial v_i}{\partial x_j}\Delta x_j. \qquad (14.1.11)$$

We add and subtract $\frac{1}{2}(\partial v_j/\partial x_i)\,\Delta x_j$ on the right side of this expression to obtain

$$\Delta v_i = \frac{1}{2}\left(\frac{\partial v_i}{\partial x_j} - \frac{\partial v_j}{\partial x_i}\right)\Delta x_j + \frac{1}{2}\left(\frac{\partial v_i}{\partial x_j} + \frac{\partial v_j}{\partial x_i}\right)\Delta x_j. \qquad (14.1.12)$$

The first term on the right represents rigid-body rotation with no rate of deformation, whereas the second term on the right represents the flow field left after translation and rotation have been subtracted out. (We removed the translation when we considered the *difference* between velocities at neighboring points.) The second coefficient of Δx_j in (14.1.12) is the strain rate (14.1.10). We have shown that, given the components of $\dot{e}_{ij}$ at the point $\mathbf{r}$, we can specify (except for the rotation) the difference in velocity between that point and a neighboring point an infinitesimal distance $\Delta\mathbf{r}$ away.

The strain-rate tensor is related to the velocity vector in exactly the same mathematical way that the strain is related to the displacement vector. Hence a proof that $\dot{e}_{ij}$ is, in fact, a tensor could begin with our knowledge that the velocity $\mathbf{v}$ is a vector and would follow identically the steps given in Section 11.2.1b, which prove that the strain is a tensor.
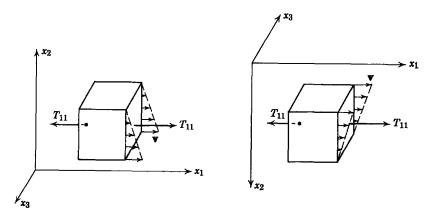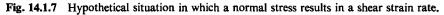
14.1.1b Stress-Strain-Rate Relations

At the beginning of this section we discussed a simple experiment that provided the relationship between the rate of shear strain and the shear stress,

$$T_{ij} = 2\mu\dot{e}_{ij}, \qquad i \neq j. \qquad (14.1.13)$$

It is possible to make a simple argument that this relation remains correct in the presence of a normal stress. Figure 14.1.7 shows a hypothetical situation in which we imagine that a normal stress T_{11} results in a strain rate $\dot{e}_{12}$. If we rotate the coordinate axes as shown in this figure, the normal stress remains unchanged in magnitude and direction but the resulting strain rate has reversed its sign. It is concluded that the rates of shear strain must be independent of the normal stresses. (This is a formal statement that, given a T_{11}, symmetry requires that the resulting rate of shear strain can be neither positive nor negative, hence must be zero.)

Fig. 14.1.7 Hypothetical situation in which a normal stress results in a shear strain rate.

Similarly, it is found that the dilatational strain rates depend only on the normal stresses. If k_1 and k_2 are experimentally determined constants, then

$$\dot{e}_{11} = k_1 T_{11} - k_2(T_{22} + T_{33}),$$
$$\dot{e}_{22} = k_1 T_{22} - k_2(T_{11} + T_{33}), \qquad (14.1.14)$$
$$\dot{e}_{33} = k_1 T_{33} - k_2(T_{22} + T_{11}).$$

A dilatational strain-rate $\dot{e}_{11}$ is shown in Fig. 14.1.8. Intuitively, we expect this type of flow to be caused by the stresses T_{11}, as shown in Fig. 14.1.8a,
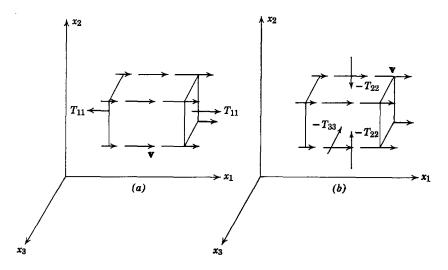

Fig. 14.1.8 Example of a dilatational strain rate showing two possible normal stresses.

or by normal stresses T_{22} and T_{33}, probably reversed in sign and not neces-
sarily with the same magnitude as T_{11}. From symmetry we expect T_{22} and
T_{33} to have an equivalent effect on the strain rate $\dot{e}_{11}$, so that there are only
two constants in each of the relations (14.1.14). Because the fluid is isotropic,
the equations must have the same form for strain-rate in each of the axis
directions.

Again, a simple argument shows that shear stresses should not appear
in (14.1.14). Suppose that a shear stress T_{12} resulted in a normal strain rate $\dot{e}_{11}$,
as shown in Fig. 14.1.9. A change of coordinates generated by rotating the
original system about a 45° axis in the x_1-x_2 plane results in a fluid element
subject to the same shear stress but displaying a strain rate $\dot{e}_{22}$ (as viewed in
the first coordinate system) rather than $\dot{e}_{11}$. Symmetry and the isotropy of the
fluid require that the dilatational strain rates depend only on the normal
stresses.

A simple example is now used to illustrate that the experimentally deter-
mined constants k_1 and k_2 in (14.1.14) are not independent of the coefficient
μ in (14.1.13).

Example 14.1.1.   A fluid is subject to a stress $T_{12} = T_{21} = T_o$ in the x_1, x_2, x_3-coordinate
system. Show that the stress and strain rate in a coordinate system x_1', x_2', x_3' defined by
$x_i' = a_{ij}x_j$, where

$$a_{ij} = \begin{bmatrix} \dfrac{1}{\sqrt{2}} & \dfrac{1}{\sqrt{2}} & 0 \\[2mm] \dfrac{-1}{\sqrt{2}} & \dfrac{1}{\sqrt{2}} & 0 \\[2mm] 0 & 0 & 1 \end{bmatrix}, \qquad \text{(a)}$$

have only normal terms and find the relation between $k_1, k_2,$ and μ that must therefore exist.

Equation 14.1.13 shows that

$$\dot{e}_{12} = \dot{e}_{21} = \frac{T_o}{2\mu}, \qquad \text{all other components} = 0 \qquad \text{(b)}$$

Because the stress and strain rate are tensors, we can find them as expressed in the $x_1', x_2',$
x_3'-coordinate system by using the transformations

$$T_{ij}' = a_{ik}a_{jl}T_{kl},$$
$$\dot{e}_{ij}' = a_{ik}a_{jl}\dot{e}_{kl}. \qquad \text{(c)}$$

Hence we find that

$$T_{ij}' = \begin{bmatrix} T_o & 0 & 0 \\ 0 & -T_o & 0 \\ 0 & 0 & 0 \end{bmatrix}, \qquad \dot{e}_{ij}' = \begin{bmatrix} \dfrac{T_o}{2\mu} & 0 & 0 \\[2mm] 0 & -\dfrac{T_o}{2\mu} & 0 \\[2mm] 0 & 0 & 0 \end{bmatrix}. \qquad \text{(d)}$$
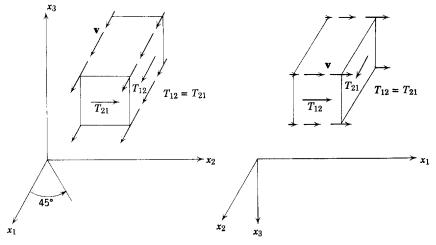
Fig. 14.1.9 Hypothetical situation in which a shear stress results in a dilatational strain rate.

It follows from these equations and (14.1.14) that

$$\dot{e}_{11}' = \frac{T_o}{2\mu} = k_1 T_o + k_2 T_o \quad \text{or} \quad k_1 + k_2 = \frac{1}{2\mu}, \qquad (e)$$

which is the desired relationship between μ, k_1, and k_2.

14.1.1c   The Equations of Fluid Dynamics as Modified by Viscosity

Equations 14.1.14 allow us to find the stress components T_{11}, T_{22}, and T_{33} in terms of the strain-rate components $\dot{e}_{11}$, $\dot{e}_{22}$, and $\dot{e}_{33}$. This result and (14.1.13) provide a concise expression for the viscous stress in terms of the strain rates:

$$T_{ij} = 2\mu(\dot{e}_{ij}) + \alpha\delta_{ij}\dot{e}_{kk}. \qquad (14.1.15)$$

We have used (e) in Example 14.1.1 to define the experimentally determined constant α in terms of the constants k_1 and k_2:

$$\alpha = \frac{k_2}{(k_1 + k_2)(k_1 - 2k_2)}. \qquad (14.1.16)$$

The numbers μ and α are physical constants that characterize the viscous properties of a fluid. The constant α, however, will not be found in the literature but rather a constant, which is a linear combination of α and μ, is defined as the *second coefficient of viscosity* η.*

$$\eta = \alpha + \tfrac{2}{3}\mu. \qquad (14.1.17)$$

* See, for example, K. F. Herzfeld and T. A. Litovitz, *Absorption and Dispersion of Ultrasonic Waves*, Academic, New York, 1959, pp. 353–361.

Reference to (14.1.10) shows that

$$\dot{e}_{kk} = \frac{\partial v_k}{\partial x_k} = \nabla \cdot \mathbf{v}; \tag{14.1.18}$$

thus the second coefficient of viscosity affects dilatational motion and has a damping effect on longitudinal disturbances (acoustic waves).

As stated earlier, we shall restrict our treatment of viscosity to examples with incompressible fluid models for which $\nabla \cdot \mathbf{v} = 0$. Thus (14.1.15) is simplified to the form

$$T_{ij} = 2\mu\dot{e}_{ij}. \tag{14.1.19}$$

Equation 14.1.19 is that part of the stress on an element of incompressible fluid created by viscous effects. The total stress of mechanical origin must include the hydrostatic pressure p [see (12.1.34)] and may be written as

$$T_{ij}{}^m = -\delta_{ij}p + \mu\left(\frac{\partial v_i}{\partial x_j} + \frac{\partial v_j}{\partial x_i}\right). \tag{14.1.20}$$

We now use this stress tensor to write the conservation of momentum for an incompressible fluid in a form that includes the viscous force density [see (12.1.14), (12.1.15), and (12.1.19)]:

$$\rho\frac{Dv_i}{Dt} = F_i{}^e + \rho g_i - \frac{\partial p}{\partial x_i} + \mu\frac{\partial}{\partial x_j}\left(\frac{\partial v_i}{\partial x_j} + \frac{\partial v_j}{\partial x_i}\right). \tag{14.1.21}$$

The order of partial differentiation is immaterial; thus

$$\frac{\partial}{\partial x_j}\left(\frac{\partial v_j}{\partial x_i}\right) = \frac{\partial}{\partial x_i}\left(\frac{\partial v_j}{\partial x_j}\right) = \frac{\partial}{\partial x_i}(\nabla \cdot \mathbf{v}),$$

which is zero for an incompressible fluid. Consequently, (14.1.21) assumes the simpler form

$$\rho\frac{Dv_i}{Dt} = F_i{}^e + \rho g_i - \frac{\partial p}{\partial x_i} + \mu\frac{\partial}{\partial x_j}\left(\frac{\partial v_i}{\partial x_j}\right). \tag{14.1.22}$$

In vector form this equation is

$$\rho\frac{D\mathbf{v}}{Dt} = \mathbf{F}^e + \rho\mathbf{g} - \nabla p + \mu\,\nabla^2\mathbf{v}. \tag{14.1.23}$$

Equation 14.1.22 or 14.1.23 is called the *Navier-Stokes equation* of fluid mechanics; for an incompressible fluid this force equation is used with a conservation of mass equation to describe the fluid dynamics. Of course, boundary conditions and the force density of electric origin $\mathbf{F}^e$ must be known.
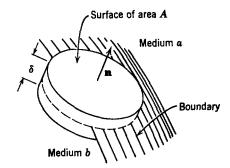
Fig. 14.1.10 Geometry for deriving boundary conditions.

14.1.2 Boundary Conditions

We specify that a boundary exists between media a and b, as illustrated in Fig. 14.1.10. The unit vector $\mathbf{n}$, which is normal to the boundary, is positive from medium b to medium a and has components n_1, n_2, and n_3 in the cartesian coordinate system x_1, x_2, and x_3. Subscripts a and b are used to denote parameters and variables in the two media.

In order for the boundary to separate the two media, the velocities at the boundary must satisfy the relation

$$\mathbf{n} \cdot \mathbf{v}_a = \mathbf{n} \cdot \mathbf{v}_b = v_n. \tag{14.1.24}$$

This merely states that the normal component of velocity must be continuous at the boundary. Furthermore, the fluid particles at the boundary must have the same normal component of velocity as the boundary; otherwise the media are interdiffusing or they are moving apart. The result of (14.1.24) can be derived formally from the conservation of mass.

We now define a right circular cylindrical volume V with end surfaces of area A and height δ, as illustrated in Fig. 14.1.10. The volume V is assumed to be small enough that in its vicinity the boundary is essentially plane. The volume is oriented so that the ends of area A are parallel to the boundary and the boundary intersects the volume as illustrated in Fig. 14.1.10. We make the further restriction that δ be so small that the lateral area of the cylindrical surface will be much smaller than the area A.

We use the conservation of momentum as expressed by (12.1.21)

$$\rho \frac{Dv_i}{Dt} = \frac{\partial T_{ij}}{\partial x_j} \tag{14.1.25}$$

to integrate throughout the volume V:

$$\int_V \rho \frac{Dv_i}{Dt}\, dV = \int_V \frac{\partial T_{ij}}{\partial x_j}\, dV = \oint_S T_{ij} n_j \, da. \tag{14.1.26}$$

When we let the volume V go to zero, the restriction of finite mass density and finite acceleration makes the left side zero. The result is

$$0 = (T_{ij}{}^a - T_{ij}{}^b)n_j. \qquad (14.1.27)$$

This expression states that the traction $(T_{ij}n_j)$ must be continuous at a surface.

Another type of boundary condition that must be specified is the condition that holds for a viscous fluid in contact with a solid surface. This situation is depicted in two dimensions in Fig. 14.1.11. We select our coordinate system so that the normal **n** to the surface is in the x_2-direction and the velocity of the fluid parallel to the boundary is in the x_1-direction. We assume no externally applied body forces (no electromagnetic or gravity forces). The condition in (14.1.24) indicates that the fluid adjacent to the boundary can have no normal component

$$v_2 = 0. \qquad (14.1.28)$$

The condition in (14.1.27) indicates that the traction at the surface must be continuous:

$$\tau_1{}^b = \mu \frac{\partial v_1}{\partial x_2}, \qquad (14.1.29a)$$

$$\tau_2{}^b = -p, \qquad (14.1.29b)$$

$$\tau_3{}^b = 0. \qquad (14.1.29c)$$

Equation 14.1.29b gives the normal component of traction on the solid surface due to the fluid, and it is just the negative of the pressure. Equation 14.1.29a gives the tangential component of traction due to the fluid. Thus, if we know how v_1 varies with x_2, we can calculate the viscous stress transmitted to the solid surface.

Although (14.1.29a) expresses the derivative of the velocity at the boundary, we also need to know the velocity at the boundary. We specify that the relative tangential velocity at the boundary is zero,

$$(\mathbf{v}_a - \mathbf{v}_b) \times \mathbf{n} = 0, \qquad (14.1.30)$$

where $\mathbf{v}_a$ is the velocity of the fluid and $\mathbf{v}_b$ is the velocity of the boundary. The physical reasoning to justify this condition is as follows: a viscous fluid
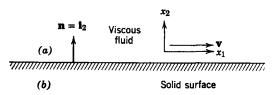

Fig. 14.1.11   A boundary between a viscous fluid and a solid surface.

exhibits friction when it flows along a solid surface, although this surface friction may have a different constant than the bulk coefficient of viscosity. If there were any tangential slippage at the boundary, it would represent an impulse in $(\partial v_1/\partial x_2)$ at the boundary, and with a finite friction coefficient it would require an infinite surface shear force. We conclude that there can be no slippage between a viscous fluid and a solid boundary.

14.1.3   Fluid-Mechanical Examples

Now that we have established the momentum equation and boundary conditions that describe incompressible viscous fluid flow it is appropriate to study some fluid flow examples without electromechanical coupling to establish ideas concerning the principal effects of viscosity that will show up later in electromechanical examples.

We consider again the example introduced in Section 14.1.1. The system is shown in Fig. 14.1.12. A viscous fluid is constrained between two parallel rigid plates separated by a distance d. The lower plate is fixed and the upper plate is made to move in the x_1-direction with constant velocity v_o. The fluid can be considered homogeneous and incompressible, $\nabla \cdot \mathbf{v} = 0$, and has a coefficient of viscosity μ. The hydrostatic pressure is constrained to be constant throughout the fluid, the system is in the steady state, and the plates are large enough in the x_1- and x_3-directions that we can neglect edge effects. Neglect the force of gravity. We want to find all components of velocity between the plates and the tangential traction applied to the plates by the fluid.

From (14.1.23), the momentum equation is:

$$\rho(\mathbf{v} \cdot \nabla)\mathbf{v} = \mu\nabla^2\mathbf{v}.$$

The upper plate is driven in the x_1-direction so we expect that $v_3 = 0$. Furthermore, the large dimensions in the x_1 and x_3 directions allow us to assume
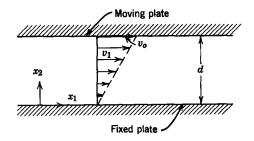
$$\partial/\partial x_1 = \partial/\partial x_3 = 0.$$

Fig. 14.1.12   A simple example of shear flow.

The use of these assumptions with $\nabla \cdot \mathbf{v} = 0$ and the boundary condition at $x_2 = \pm d$ yield

$$v_2 = 0.$$

The momentum equation thus reduces to

$$0 = \frac{\partial^2 v_1}{\partial x_2{}^2}.$$

Integration of this equation twice yields:

$$v_1 = C_1 x_2 + C_2.$$

The requirement of continuous tangential velocity at a boundary (14.1.30) gives

$$\text{at} \quad x_2 = 0, \quad v_1 = 0, \quad C_2 = 0,$$

$$\text{at} \quad x_2 = d, \quad v_1 = v_o, \quad C_1 = \frac{v_o}{d}.$$

Thus

$$v_1 = v_o \frac{x_2}{d}.$$

This profile, referred to as *plane Couette flow*, is sketched in Fig. 14.1.12.
The use of (14.1.27) yields for the tangential component of traction

$$\text{at} \quad x_2 = 0, \quad \tau_1 = \mu \frac{v_o}{d},$$

$$\text{at} \quad x_2 = d, \quad \tau_1 = -\mu \frac{v_o}{d}.$$

It is apparent that the viscous traction tends to oppose the relative motion of the two plates as we intuitively expected.

The type of flow described in this example is used in a device specifically designed to measure the coefficient of viscosity. It consists of two concentric cylinders with a small annular space between them. One cylinder is fixed and the other can be rotated about its axis. The fluid is introduced into the space between the cylinders, and the torque required to rotate one cylinder at a particular speed is measured. This torque is used with the known lever arm and the expression for surface traction to calculate the viscosity.

As a second example, consider the pressure-driven, steady flow of an incompressible viscous fluid between two fixed parallel plates separated by a distance *2d*, as illustrated in Fig. 14.1.13. The lateral extent of the plates
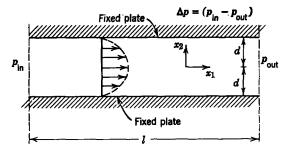
Fig. 14.1.13 Two-dimensional viscous flow.

is large enough compared with $2d$ that we can neglect edge effects. We orient our coordinate axes x_1 and x_2 so that there is no flow or variation of velocity along x_3. We assume that there is only an x_1-component of velocity and show that this satisfies the differential equations and the boundary conditions.

In this case our assumptions are

$$v_2 = v_3 = 0, \qquad \frac{\partial}{\partial x_3} = 0.$$

With these assumptions $\nabla \cdot \mathbf{v} = 0$ reduces to

$$\frac{\partial v_1}{\partial x_1} = 0, \tag{14.1.31}$$

and we can write the x_1-component of (14.1.22) as

$$0 = -\frac{\partial p}{\partial x_1} + \mu \frac{\partial^2 v_1}{\partial x_2^2}. \tag{14.1.32}$$

When we take the partial derivative of this expression with respect to x_1 and use (14.1.31), we find

$$\frac{\partial^2 p}{\partial x_1^2} = 0, \tag{14.1.33}$$

which shows that $\partial p / \partial x_1$ is constant. Setting

$$\frac{\partial p}{\partial x_1} = -\frac{\Delta p}{l}, \tag{14.1.34}$$

where Δp is the pressure difference impressed across the length l in the x_1-direction (the pressure decreases with x_1 so that the flow is in the positive x_1-direction), we can write (14.1.32) as

$$\mu \frac{\partial^2 v_1}{\partial x_2^2} = -\frac{\Delta p}{l}. \tag{14.1.35}$$

Integrating this expression twice with respect to x_2 yields

$$v_1 = -\frac{\Delta p}{2\mu l} x_2{}^2 + C_1 x_2 + C_2. \qquad (14.1.36)$$

We first use the symmetry condition that $dv_1/dx_2 = 0$ at $x_2 = 0$ to set $C_1 = 0$. We then use the boundary conditions that $v_1 = 0$ at $x_2 = \pm d$ to obtain

$$C_2 = \frac{\Delta p\, d^2}{2\mu l}.$$

The final result, referred to as *plane Poiseuille flow*, is

$$v_1 = \frac{\Delta p}{2\mu l} (d^2 - x_2{}^2). \qquad (14.1.37)$$

The parabolic velocity profile indicated by (14.1.37) is sketched in Fig. 14.1.13. It can be shown by direct substitution that this solution also satisfies the x_2- and x_3-components of (14.1.22).

14.2 ELECTROMECHANICAL COUPLING WITH VISCOUS FLUIDS

To illustrate in simple contexts how viscosity affects electromechanical coupling and vice versa we reconsider the two examples of the preceding section with electromechanical coupling added. In both cases we apply magnetic fields and assume that the fluids have high enough electrical conductivity that a quasi-static magnetic field system is the appropriate electromagnetic model.

14.2.1 Electromechanical Coupling with Shear Flow

The system to be analyzed is shown in Fig. 14.2.1b. It consists of two parallel, highly conducting plates, separated by an incompressible conducting liquid with conductivity σ and coefficient of viscosity μ. The plates and liquid are both nonmagnetic. The lower plate is fixed and the upper plate is moving with velocity v_o in the x_1-direction. A uniform flux density B_o is applied (by a system not shown) in the x_3-direction and a uniform current density J_o is injected in the x_2-direction. The system is operating in the steady state ($\partial/\partial t = 0$). This is a representation of a liquid metal brush like those used in the acyclic generator of Fig. 6.4.13. (See Fig. 14.2.1a.) Our use of a plane geometry is a simplification based on the fact that the thickness d of the fluid is very small compared with the radius of curvature. Our analysis allows assessment of the effect of B_o on the characteristics of the brush, primarily the voltage drop of the brush and the losses, both electrical and mechanical, that heat the fluid.
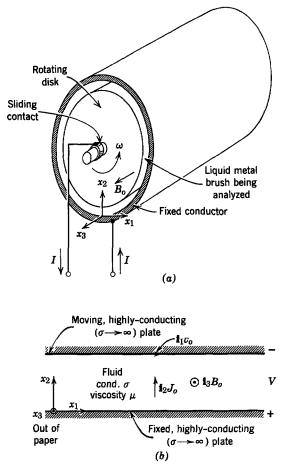
Fig. 14.2.1   Configuration for analyzing the effect of electromechanical coupling on shear flow. (a) physical system, (b) mathematical approximation.

Recognizing that this planar model is a representation of an annular system that closes on itself in the x_1-direction and that the system is symmetrical, we conclude that no properties can vary with x_1; thus

$$\frac{\partial}{\partial x_1} = 0.$$

Furthermore, the system is large enough in the x_3-direction that we can neglect end effects. The current paths external to the fluid close in such a way that the field induced by current density J_o according to Ampère's law is only in the x_1-direction. With these assumptions about the system

we can specify the relevant variables as

$$\mathbf{v} = \mathbf{i}_1 v_1(x_2), \qquad \mathbf{J} = \mathbf{i}_2 J_o \qquad (14.2.1)$$
$$\mathbf{E} = \mathbf{i}_2 E_2(x_2), \qquad \mathbf{B} = \mathbf{i}_3 B_o + \mathbf{i}_1 B_1(x_3).$$

These explicit functional dependences will be shown to satisfy the relevant differential equations and boundary conditions as the analysis proceeds.

With the variables defined above and the restrictions cited earlier, the x_1-component of the momentum equation (14.1.22) is

$$0 = J_o B_o + \mu \frac{\partial^2 v_1}{\partial x_2{}^2}. \qquad (14.2.2)$$

The quantities J_o, B_o, and μ are constants and v_1 varies only with x_2; consequently, (14.2.2) is integrated twice to obtain

$$v_1 = -\frac{J_o B_o}{2\mu} x_2{}^2 + C_1 x_2 + C_2, \qquad (14.2.3)$$

where C_1 and C_2 are constants of integration to be determined by boundary conditions. The boundary condition of (14.1.30) which requires no slippage yields

$$\text{at} \quad x_2 = 0, \qquad v_1 = 0,$$
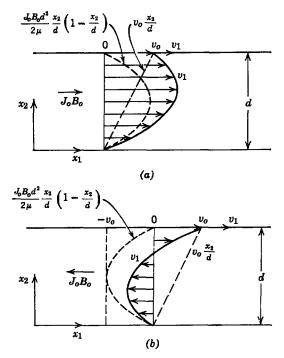$$\text{at} \quad x_2 = d, \qquad v_1 = v_o.$$

The use of these two conditions to evaluate C_1 and C_2 in (14.2.3) leads to the resulting velocity

$$v_1 = v_o \frac{x_2}{d} + \frac{J_o B_o d^2}{2\mu} \frac{x_2}{d}\left(1 - \frac{x_2}{d}\right). \qquad (14.2.4)$$

The first term is just the linear variation obtained in Fig. 14.1.12 with no electromechanical coupling. The second term is a parabolic profile that results from the electromechanical coupling. The second term can be positive or negative, depending on the sign of the product $J_o B_o$. The two terms in (14.2.4) are sketched with the composite profile for two conditions in Fig. 14.2.2. The $\mathbf{J} \times \mathbf{B}$ force density in the x_1-direction is uniform; consequently, the parabolic profile is expected from the results of the second example of Section 14.1.3, which was driven by a constant force density due to a pressure gradient (see Fig. 14.1.13). It is clear from Fig. 14.2.2 that the magnetic force can have a marked effect on the profile, even reversing the velocity in Fig. 14.2.2b. The profiles indicate more shear strain rate with the magnetic force than without; thus, as we shall see subsequently, we can expect increased fluid mechanical losses.

At this point it is well to note that there is an x_3 component of $\mathbf{J} \times \mathbf{B}$ ($J_o B_1$). Because B_1 is excited by J_o it depends only on x_3, thus the x_3 component

Fig. 14.2.2 Velocity profiles resulting from uniform magnetic force density applied to shear flow. The profiles are sketched for $|J_o B_o| = 8\mu v_o/d^2$: (a) $J_o B_o > 0$, $\mathbf{J} \times \mathbf{B}$ force density is in direction of v_o; (b) $J_o B_o < 0$, $\mathbf{J} \times \mathbf{B}$ force density is opposite to v_o.

of force density depends only on x_3. With end seals on the brush there can be no flow in the x_3 direction and the force density is balanced by a pressure gradient in the x_3 direction. This pressure variation will not affect the flow pattern because the fluid is incompressible.

To evaluate the system of Fig. 14.2.1 for use as a liquid metal brush for carrying current from a fixed to a moving member we must evaluate the voltage across the brush, the mechanical force needed to maintain the steady motion, and the total power input to the brush that must be removed by heat transfer to maintain acceptable brush temperature in the steady state.

Voltage V has the polarity defined in Fig. 14.2.1, and is related to the electric field intensity by

$$V = \int_0^d E_2 \, dx_2. \tag{14.2.5}$$

Ohm's law for a moving fluid (12.2.18) yields

$$E_2 = \frac{J_o}{\sigma} + v_1 B_o. \tag{14.2.6}$$

The use of this expression, with (14.2.4) for v_1, in (14.2.5) and evaluation of the integral lead to

$$V = \frac{J_o}{\sigma} d + B_o v_o \frac{d}{2} + \frac{J_o B_o^2 d^3}{12\mu}. \tag{14.2.7}$$

The first term is just the voltage that results with J_o in the fluid at rest. The second term can be interpreted as the speed voltage generated by the linear velocity variation of simple shear flow (see Fig. 14.2.2). The last term is the speed voltage generated by the parabolic velocity profile of Fig. 14.2.2.

The electrical power input p_e per unit area in an x_1-x_3-plane is found by taking the product

$$p_e = J_o V = \frac{J_o^2}{\sigma} d + J_o B_o v_o \frac{d}{2} + \frac{J_o^2 B_o^2 d^3}{12\mu}. \tag{14.2.8}$$

The first and third terms are always positive, but the second term can be negative, in which case the brush can act as an MHD generator and produce net electrical power. This is not a practical source of power, but it does indicate the nature of possible electrical characteristics of liquid metal brushes in the presence of a magnetic field.

The traction (force per unit area) that must be applied to the upper plate to maintain the steady motion is found from (14.1.29a) to be

$$\tau_1 = \mu \frac{\partial v_1}{\partial x_2}\bigg|_{x_2=d}. \tag{14.2.9}$$

The use of (14.2.4) in this expression yields

$$\tau_1 = \mu \frac{v_o}{d} - \frac{J_o B_o d}{2}. \tag{14.2.10}$$

The second term is negative because, as indicated in Fig. 14.2.2a, the $\mathbf{J} \times \mathbf{B}$ force drives the fluid faster and tries to accelerate the upper plate, thus requiring a negative component of traction to maintain steady velocity.

The mechanical input power p_m per unit area is found as

$$p_m = \tau_1 v_o = \mu \frac{v_o^2}{d} - \frac{J_o B_o v_o d}{2}. \tag{14.2.11}$$

Once again the brush may actually produce net mechanical power.

To find the total power per unit area p_t put into the brush electrically and mechanically we add (14.2.8) and (14.2.11) to obtain the result.

$$p_t = p_e + p_m = \frac{J_o^2}{\sigma} d + \mu \frac{v_o^2}{d} + \frac{J_o^2 B_o^2 d^3}{12\mu}. \tag{14.2.12}$$

The total power input is always positive, even though (14.2.8) and (14.2.11) indicate that there may be net electrical output or net mechanical output.

In (14.2.12) the first term is simply the Joule loss associated with current in the conducting fluid; the second term is the viscous loss that would result from simple shear flow; and the third term results from the electromechanical coupling.

It should be clear from the form of (14.2.12) that for a system in which the quantities σ, μ, J_o, v_o, and B_o are known there is a brush thickness that minimizes brush losses. This optimum brush thickness can be found by a straightforward application of differential calculus. We shall not carry out this process here. Rather, we shall assume liquid metal brush parameters typical of configurations used in practice and compare the brush properties with those of carbon brushes. At the same time we shall assess the effects of electromechanical coupling on the liquid metal brush.

The parameters assumed for the liquid metal brush are given in Table 14.2.1. Substitution of these quantities into (14.2.7) and (14.2.12) yields

$$V = 0.015 + 0.15B_o + 83.3B_o{}^2 \text{ V},$$

$$p_t = 2.26 \times 10^4 + 1.25 \times 10^8 B_o{}^2 \text{ W/m}^2.$$

Table 14.2.1   Parameters Assumed for Liquid Metal Brush

Material	Mercury
Conductivity	$\sigma = 10^6$ mhos/m
Viscosity	$\mu = 1.5 \times 10^{-3}$ kg/m-sec
Current density	$J_o = 1.5 \times 10^6$ A/m^2
Velocity	$v_o = 30$ m/sec
Brush thickness	$d = 10^{-2}$ m

These two quantities are plotted on logarithmic scales as functions of flux density B_o in Fig. 14.2.3. The characteristics of a metal-graphite brush of the type normally used for slip rings* are also shown. The metal-graphite brush operates at only *one tenth* the current density of the liquid metal brush; thus for the same total current the solid brush will require 10 times as much contact area. At very low flux density the liquid metal brush has a voltage drop roughly two orders of magnitude lower than that of a solid brush, and the power loss per unit area is three orders of magnitude lower. When the flux density gets to the range of 0.1 to 1 Wb/m² the liquid metal brush performance deteriorates rapidly as flux density increases. The curves of Fig. 14.2.3 demonstrate clearly the superiority of liquid metal brushes with respect to contact drop and losses, but they also demonstrate that magnetic fields can degrade the liquid metal brush performance markedly.

In this example we have demonstrated how electromechanical coupling

---

* The characteristics of the metal-graphite brush were taken from *Standard Handbook for Electrical Engineers*, A. E. Knowlton, ed., McGraw-Hill, New York, 9th ed., 1957, Sections 4-234 and 8-120.
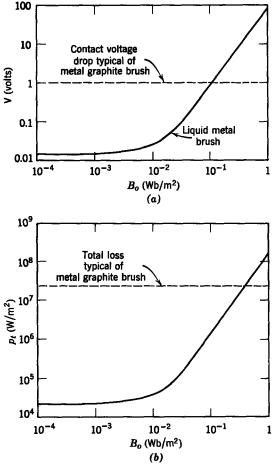
Fig. 14.2.3 Voltage and brush loss as functions of applied flux density for liquid metal brushes compared with metal graphite brushes: (a) brush voltage; (b) total brush loss.

can have a considerable effect on the behavior of a fluid mechanical system in a configuration of practical significance. In the next section we treat another configuration in which electromechanical coupling can have significant effects.

14.2.2 Electromechanical Coupling with Pressure-Driven Flow (Hartmann Flow)

In this section we consider the effects of viscosity on fluid flow in a rectangular channel. The electrical conductivity of the fluid is high enough to justify a magnetic field system model and the fluid is subjected to transverse magnetic field and current. Thus this example allows us to assess the effects
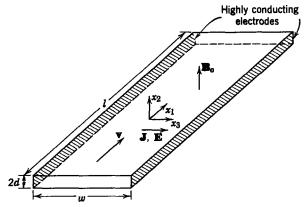
Fig. 14.2.4 Configuration for studying Hartmann flow.

of viscosity on the conduction-type MHD machines considered in Chapters 12 and 13 and to determine the conditions under which the inviscid fluid models used there are accurate.

The flow pattern to be analyzed is conventionally called *Hartmann flow* and will be studied in the configuration of Fig. 14.2.4. The channel has a length l, a width w, and a depth $2d$. The aspect ratio of the channel is quite large

$$\frac{w}{2d} \gg 1,$$

and we are interested in the flow properties near the center of the channel. Thus we can neglect variations with x_3. The sides of the channel that lie in the x_1-x_2 planes are highly conducting electrodes and can be connected to an external circuit with the result that there can be net current flow across any x_1-x_2 plane.

The fluid is assumed to be incompressible with coefficient of viscosity μ and electrical conductivity σ. There is an applied flux density $\mathbf{B}_o$,

$$\mathbf{B}_o = \mathbf{i}_2 B_o, \tag{14.2.13}$$

and we assume that the magnetic flux density due to current flow in the fluid is negligible compared to B_o (low magnetic Reynolds number). We also assume steady flow.

We neglect end effects, and thus we are considering the two-dimensional problem in Fig. 14.2.5. The symmetry of the simplified problem allows us to assume the following forms for the variables:

$$\mathbf{v} = \mathbf{i}_1 v_1(x_2), \tag{14.2.14a}$$

$$\mathbf{E} = \mathbf{i}_3 E_3(x_2), \tag{14.2.14b}$$

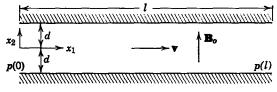$$\mathbf{J} = \mathbf{i}_3 J_3(x_2). \tag{14.2.14c}$$

Fig. 14.2.5 Two-dimensional configuration for Hartmann flow.

All of these variables are functions of x_2 only, as indicated. It should be clear at this point that our example is simply the one shown in Fig. 14.1.13 with the addition of a magnetic force density. Thus we expect our result to be similar to and interpretable in terms of the results given in Fig. 14.1.13. From Faraday's law (1.1.5)* we obtain

$$\frac{dE_3}{dx_2} = 0,$$ (14.2.15)

from which we obtain

$$E_3 = \text{constant.}$$ (14.2.16)

The x_3-component of Ohm's law, (12.2.18) is

$$J_3 = \sigma(E_3 + v_1 B_o).$$ (14.2.17)

The x_1-component of the momentum equation (14.1.22) is

$$0 = -\frac{\partial p}{\partial x_1} + \mu \frac{d^2 v_1}{dx_2{}^2} - J_3 B_o.$$ (14.2.18)

Recognizing that J_3 and v_1 are not functions of x_1, we differentiate (14.2.18) with respect to x_1 to obtain

$$\frac{\partial^2 p}{\partial x_1{}^2} = 0,$$ (14.2.19)

which shows that

$$\frac{\partial p}{\partial x_1} = \text{constant.}$$ (14.2.20)

Denoting the pressure drop over the length of the channel as Δp,

$$\Delta p = p(0) - p(l),$$ (14.2.21)

we can write (14.2.20)

$$\frac{\partial p}{\partial x_1} = -\frac{\Delta p}{l}.$$ (14.2.22)

Compare these results with (14.1.33) and (14.1.34). We assume that Δp is

* Table 1.2, Appendix G.

maintained constant by external means; thus it represents an independent input to the system.

We now substitute (14.2.17) and (14.2.22) in (14.2.18) and rearrange the resulting expression to obtain

$$\frac{d^2 v_1}{dx_2^{\ 2}} - \frac{\sigma B_o^{\ 2}}{\mu} v_1 = -\frac{\Delta p}{\mu l} + \frac{\sigma B_o E_3}{\mu}. \qquad (14.2.23)$$

Equation 14.2.16 indicates that E_3 is constant; thus we can solve this linear differential equation with constant coefficients to obtain, in general,

$$v_1 = C_1 \sinh M \frac{x_2}{d} + C_2 \cosh M \frac{x_2}{d} + \frac{\Delta p}{\sigma B_o^{\ 2} l} - \frac{E_3}{B_o}, \qquad (14.2.24)$$

where we have defined the *Hartmann number* M as

$$M = B_o d \left(\frac{\sigma}{\mu}\right)^{1/2}. \qquad (14.2.25)$$

We must now apply the boundary condition that at

$$x_2 = \pm d, \qquad v_1 = 0. \qquad (14.2.26)$$

This imposes the requirement that v_1 be an even function of x_2; thus

$$C_1 = 0, \qquad (14.2.27)$$

and the constant C_2 is then given by

$$C_2 = \frac{-1}{\cosh M} \left(\frac{\Delta p}{\sigma B_o^{\ 2} l} - \frac{E_3}{B_o}\right). \qquad (14.2.28)$$

We now use (14.2.27) and (14.2.28) to write (14.2.24) as

$$v_1 = \left(\frac{\Delta p}{\sigma B_o^{\ 2} l} - \frac{E_3}{B_o}\right) \left[1 - \frac{\cosh M(x_2/d)}{\cosh M}\right]. \qquad (14.2.29)$$

To complete the solution for the velocity profile we must specify the value of the electric field E_3. We can fix E_3 by the application of a terminal voltage as we did in Section 12.2.1a. Alternatively, we can fix E_3 by constraining the total current that can flow across an x_1-x_2 plane. To complete the present example we assume that the external terminals are open-circuited; the result is no net current across an x_1-x_2 plane. Mathematically, this requirement can be written as

$$\int_{-d}^{d} J_3 \, dx_2 = 0. \qquad (14.2.30)$$

We use (14.2.17) with this expression to obtain

$$E_3 = - \frac{B_o}{2d} \int_{-d}^{d} v_1 \, dx_2. \tag{14.2.31}$$

We now use (14.2.29) in (14.2.31), evaluate the integral, and solve for E_3 to obtain

$$E_3 = - \frac{\Delta p}{\sigma l B_o} \left(\frac{M \cosh M - \sinh M}{\sinh M} \right). \tag{14.2.32}$$

Substitution of (14.2.32) into (14.2.29) and simplification yield

$$v_1 = \frac{\Delta p}{\sigma B_o^2 l} \left\{ \frac{M[\cosh M - \cosh M(x_2/d)]}{\sinh M} \right\}. \tag{14.2.33}$$

It will be easy to interpret our results if we assume that the mechanica properties are fixed and vary the applied magnetic field to vary M. For this purpose it is more useful to write (14.2.33) in the form

$$v_1 = \frac{\Delta p \, d^2}{\mu l} \left[\frac{\cosh M - \cosh M(x_2/d)}{M \sinh M} \right]. \tag{14.2.34}$$

As a check on this expression, it is easily verified that the limit taken as $M \to 0$ yields the same velocity profile as in the second example of Section 14.1.3 (see Fig. 14.1.13). This is as it should be, for when $M \to 0$ in (14.2.34) this profile is achieved by eliminating electrical and retaining only viscous effects.

To interpret the meaning of the profile shape of (14.2.34) we assume a system of fixed dimensions, with a fluid of fixed properties and constrain the pressure drop Δp to be fixed. We now vary the applied flux density B_o and ask how the shape of the profile changes. Such changes are indicated in Fig. 14.2.6, in which the profiles are plotted for three values of M. Note that the profile for $M = 0$ is the same as that plotted in Fig. 14.1.13.

To interpret the results of Fig. 14.2.6 we observe first that in the absence of electromagnetic forces the velocity profile is parabolic. This is the profile given with viscous effects alone. When electromagnetic forces are present, any local variation of velocity will generate circulating currents that interact with the applied magnetic field to reduce the local velocity variations. Thus the presence of the applied magnetic field tends to make the velocity uniform. When the applied magnetic field is large (M large), the velocity is uniform near the center of the channel and varies appreciably in the vicinity of the walls where the velocity must go to zero. Whether the velocity profile is flat or parabolic depends on the value of the Hartmann number M given by (14.2.25) as

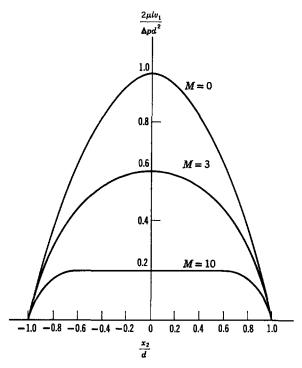$$M = B_o \, d \left(\frac{\sigma}{\mu} \right)^{\frac{1}{2}}.$$

Fig. 14.2.6 Variation of velocity profile with Hartmann number.

For low values of M viscous forces predominate and the profile tends to be parabolic. For high values of M electromagnetic forces predominate and the velocity profile tends to be flat. Thus the Hartmann number is interpreted as a measure of the relative magnitude of electromagnetic and viscous forces. It is clear that for high values of M the model of uniform flow velocity used earlier in Section 12.2.1a is valid over most of the channel width. We consider this situation subsequently with more precision.

It is evident from the curves of Fig. 14.2.6 that with a fixed pressure drop the volume flow rate of the fluid is reduced by the presence of an applied magnetic field. If we designate the volume flow rate by $\dot{V}_{ol}$, it is given by

$$\dot{V}_{ol} = w \int_{-d}^{d} v_1 \, dx_2 \text{ m}^3/\text{sec}. \qquad (14.2.35)$$

We now use (14.2.34) in this expression, perform the integration, and simplify to obtain

$$\dot{V}_{ol} = \frac{2\Delta p \, d^3 w}{3\mu l} \left[\frac{3}{M^2} (M \coth M - 1) \right]. \qquad (14.2.36)$$
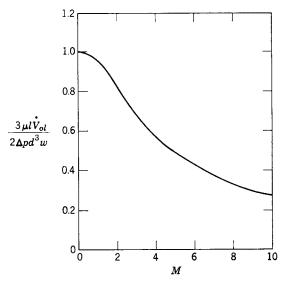
Fig. 14.2.7   Variation of volume flow rate with Hartmann number.

In the limit as $M \rightarrow 0$ the volume flow rate becomes

$$(\dot{V}_{ol})_{M=0} = \frac{2\Delta p \; d^3 w}{3\mu l},$$

which is the volume flow rate in the presence of viscous forces only. The expression of (14.2.36), normalized to the value for $M \rightarrow 0$,

$$\frac{3\mu l \dot{V}_{ol}}{2\Delta p \; d^3 w} = \frac{3}{M^2}(M \coth M - 1), \qquad (14.2.37)$$

is plotted as a function of M in Fig. 14.2.7. It is evident from the curve of Fig. 14.2.7 that the presence of a magnetic field that yields an appreciable Hartmann number will markedly reduce the volume flow rate for a given pressure drop.

To ascertain the order of magnitude of Hartmann number that can be obtained with real conducting fluids consider liquid mercury which has

$$\sigma = 10^6 \; \text{mhos/m}, \qquad \mu = 1.5 \times 10^{-3} \; \text{kg/m-sec}$$

If we consider a system with a channel depth of 2 cm,

$$d = 10^{-2} \; \text{m},$$

and an applied flux density of

$$B_o = 1 \; \text{Wb/m}^2 = 10,000 \; \text{gauss},$$

the resulting Hartmann number is

$$M = 260.$$

Thus the flow of mercury under these conditions is very strongly affected by electromagnetic forces. The same is true of other liquid metals.

Alternatively, a seeded combustion gas would be used in the variable-area channel considered in Section 13.2.2. This system would have approximately the following constants,

$$\sigma = 40 \text{ mhos/m}, \qquad \mu = 10^{-5} \text{ kg/m-sec},$$
$$B_o = 4 \text{ Wb/m}^2, \qquad d = 10^{-1} \text{ m},$$

and a Hartmann number

$$M = 800.$$

Thus, even with an ionized gas with its very small conductivity, this large Hartmann number indicates that magnetic forces predominate over viscous forces.

To be more precise about how viscosity affects a conduction-type MHD machine we remove the constraint of no net current and operate the system in Fig. 14.2.4 as we did the MHD machine in Section 12.2.1a. In the present system the channel depth is $2d$, whereas in Fig. 12.2.3 the channel depth is d. Redefining the quantities for the inviscid fluid model to account for this difference, we have [see (12.2.21), (12.2.22), and (12.2.24)] for the inviscid model

$$\text{internal resistance,} \qquad R_i = \frac{w}{2\sigma l d}, \tag{14.2.38}$$

$$\text{voltage equation,} \qquad IR_i = v_o B_o w - V, \tag{14.2.39}$$

$$\text{pressure drop,} \qquad \Delta p = \frac{IB}{2d}, \tag{14.2.40}$$

where I and V are defined in Fig. 14.2.4 and v_o is the fluid velocity for an inviscid fluid model.

We now remove the constraint of no net current (14.2.30) and instead specify that the electric field intensity be given in terms of the terminal voltage as

$$E_3 = -\frac{V}{w}. \tag{14.2.41}$$

From Ohm's law (14.2.17) the current density becomes

$$J_3 = \sigma\left(-\frac{V}{w} + v_1 B_o\right) \tag{14.2.42}$$

and the terminal current is

$$I = \int_{-d}^{d} J_3 l \, dx_2. \tag{14.2.43}$$

Substitution of (14.2.42) into (14.2.43) yields

$$I = -\frac{V}{R_i} + \sigma l B_o \int_{-d}^{d} v_1 \, dx_2. \tag{14.2.44}$$

When the space average velocity is defined

$$\langle v_1 \rangle = \frac{1}{2d} \int_{-d}^{d} v_1 \, dx_2, \tag{14.2.45}$$

we can write (14.2.44) in the form

$$IR_i = -V + B_o w \langle v_1 \rangle. \tag{14.2.46}$$

This expression is the same as (14.2.39) for the inviscid model except that v_o for the inviscid case is replaced by average velocity in the viscous case.

The most important aspect of viscosity in an MHD machine is how much of the pressure gradient goes into viscous losses and how much is balanced by the magnetic force density. To answer this question we evaluate the average velocity by using (14.2.29) in (14.2.45) to obtain

$$\langle v_1 \rangle = \left(\frac{\Delta p}{\sigma B_o^2 l} + \frac{V}{B_o w} \right) \left(1 - \frac{\tanh M}{M} \right). \tag{14.2.47}$$

The use of this result in (14.2.46) and solution for Δp yield

$$\Delta p = \frac{B_o I / 2d + (B_o \sigma l V / w)(\tanh M / M)}{1 - \tanh M / M}. \tag{14.2.48}$$

Noting that the first term in the numerator is the pressure drop in an inviscid machine, as given by (14.2.40), we write the ratio

$$\frac{\Delta p}{\Delta p_i} = \frac{1 + (V/IR_i)(\tanh M / M)}{1 - \dfrac{\tanh M}{M}}, \tag{14.2.49}$$

where Δp_i is the ideal pressure drop given by (14.2.40). This ratio is plotted as a function of Hartmann number M in Fig. 14.2.8 with

$$\frac{V}{IR_i} = 1,$$

which is the condition for maximum electrical power extraction from the flowing fluid. Note that the Hartmann number axis is a logarithmic scale.
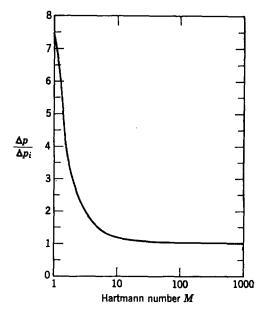
Fig. 14.2.8   Ratio of actual pressure drop and ideal pressure drop for an MHD generator loaded to extract maximum electric power.

It is clear that the error is large for a small Hartmann number with a pressure drop 22 per cent more than the ideal for $M = 10$. At $M = 100$ the error is 2 per cent, and at $M = 1000$ the error is 0.2 per cent. This shows that for a Hartmann number of the order of 100 or larger the inviscid fluid model used to analyze MHD machines in Chapters 12 and 13 is quite accurate with respect to the neglect of the effects of viscosity.
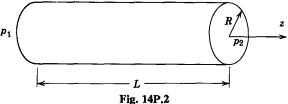
14.3   DISCUSSION

In this chapter we have added the effects of viscosity to the mathematical description of incompressible fluids. In the process we have indicated how this description is modified for compressible fluids. We have analyzed and discussed two applications of the equations to steady flow problems in which viscous effects and electromechanical coupling compete; and one or the other can predominate, depending on the relative values of the critical parameters.

It is a straightforward process to extend the techniques of this chapter to dynamic situations; for example, we can use the description of viscosity in this chapter to study viscous damping of the Alfvèn waves defined and analyzed in a lossless system in Section 12.2.3.

PROBLEMS

14.1. Rework the example of Sec. 14.2.1 with the applied flux density in the x_2 direction. Assume that no current can flow in the x_3 direction. In particular obtain expressions for velocity profile (like Eq. 14.2.4), voltage (like Eq. 14.2.7), traction (like Eq. 14.2.10), and total power per unit area (like Eq. 14.2.12). Make plots of voltage and loss per unit area for the constants of Table 14.2.1 and compare the results with those plotted in Fig. 14.2.3.

14.2. A viscous liquid flows through a circular pipe, as shown in Fig. 14P.2. At the inlet the pressure is uniform and equal to p_1, and at the outlet it is still uniform, but p_2. The volume rate of flow is $Q m^3$/sec. Under the assumption that the flow is axisymmetric and steady and that the velocity is low enough that the fluid can be considered incompressible, find the velocity profile $v_z(r)$. *Hint.* Look for solutions where $\mathbf{v} = v_z(r)\mathbf{i}_z$ and $p = p(z)$.

Fig. 14P.2

14.3. The channel shown in Fig. 14P.3 contains a viscous fluid of conductivity σ moving in the x_1-direction. You are to analyze this problem using the Hartmann flow solutions (Section 14.2.2). The highly conducting electrodes are connected by a load resistance R.

    (a) Given the pressure drop from inlet to outlet, the dimensions of the system, field B_0, and conductivity σ, what is the power dissipated in the resistance?

    (b) What value of R should be used to dissipate the largest possible power in the load?

    (c) If the fluid is mercury, $B_0 = 20,000$ gauss, $d = 1$ cm, $l = 1$ m, and $w = 10$ cm, what is the Hartmann number? What is the value of the optimum resistance found in part (b)?
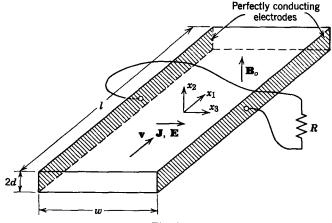

Fig. 14P.3